UNIVERSITY BABEŞ-BOLYAI
FACULTY OF PHYSICS

SUMMARY

Computational studies of donor-acceptor molecules for organic photovoltaics

Author:
Sergiu Cristian POP

Supervisor:
Prof. Dr. Titus Adrian BEU

September, 2012

Keywords: organic photovoltaics, polythiophenes, fullerenes, Density Functional Theory, Molecular Dynamics, charge transfer, Cayley algorithm

Contents

1
Introduction

The main limitation for the conventional inorganic semiconducter-based photovoltaics is the continuous cost increase for silicon, other materials involved, and the process technologies needed to build the photovoltaic modules. Over the last years, the cutting edge of the photovoltaic technology is represented by the third generation of solar cells, which include the dye-sensitized and the polymeric solar cells. They are based on π conjugated polymers due to their semiconducting properties. For example, hexathiophene was used to fabricate thin film transistors and organic photovoltaics with promising performances for large area of electronic circuits. Both doped and undoped categories exhibit a remarkable chemical and electrochemical stability in air. Physical and chemical properties of polythiophenes are generally studied either in solution or on polycrystalline thin films that can be obtained by spin coating and printing in the case of soluble compounds, or by vacuum evaporation for materials in crystalline phase.

The charge transport in organic semiconductors is sensitive to many factors, such as molecular arrangement, presence of impurities which can act as dopants or traps, etc. In order to control the morphology by optimizing the growth process, to design the energetic gaps, as well as tailoring the optical and electronic properties of thin films based on thiophene oligomers, a comprehensive study of the physical and chemical properties of the polymers is required. A central role is played by the vibrational properties, which, being most sensitive to conformational changes induced, for example, by doping, may provide important structural information susceptible to be useful in developing new applications.

2

Theoretical background

1. Molecular and lattice dynamics in organic molecular crystals
    (a) Elements of infrared spectroscopy
    (b) Elements of Raman scattering
    (c) Electron-phonon interactions
2. The Hartree-Fock Approximation
    (a) The Hartree-Fock Equations
    (b) The Rothaan Equations
3. Molecular dynamics measurements
    (a) Radial distribution function
    (b) Diffusion coefficients
4. Charge transfer in organic semiconductors
    (a) Excitons formation
    (b) Vibronic Coupling

3

Morphology studies of polythiophenes and thiophene/fullerene-based dyads

3.1 Vibrational spectroscopy

3.1.1 Vibrations of polythiophenes

The first part of the present study focuses on the accurate first principles calculation of the equilibrium structures, normal modes, and vibrational spectra of the 12 smallest polythiophene oligomers. Whereas previous works have been concerned only with even-sized molecules [1, 2], we have considered also the odd-sized ones.

All DFT calculations presented in this chapter, both structural and vibrational, have been carried out using the GAUSSIAN 03 package [3].

3.1.1.1 Geometries.

Interested in the degree to which different exchange-correlation functionals prove appropriate for the particular case of polythiophenes, we have performed comparative calculations with the B3LYP [4] and PBE [5] functionals. In geometrical terms, as seen from. Table 3.1, which lists the relative deviations of several bond lengths of hexathiophene from experimental values [1], there emerges a slightly better ability (typically amounting to 0.01 Å) of the B3LYP functional to reproduce the inter-cycle C-C bond [6, 7] and C-S bonds [8]. On the other hand, the PBE-based calculations provided closer agreement with the experiments for the in-ring double C=C bonds and the bonds in between, particularly for the ones opposed to the sulphur atoms.

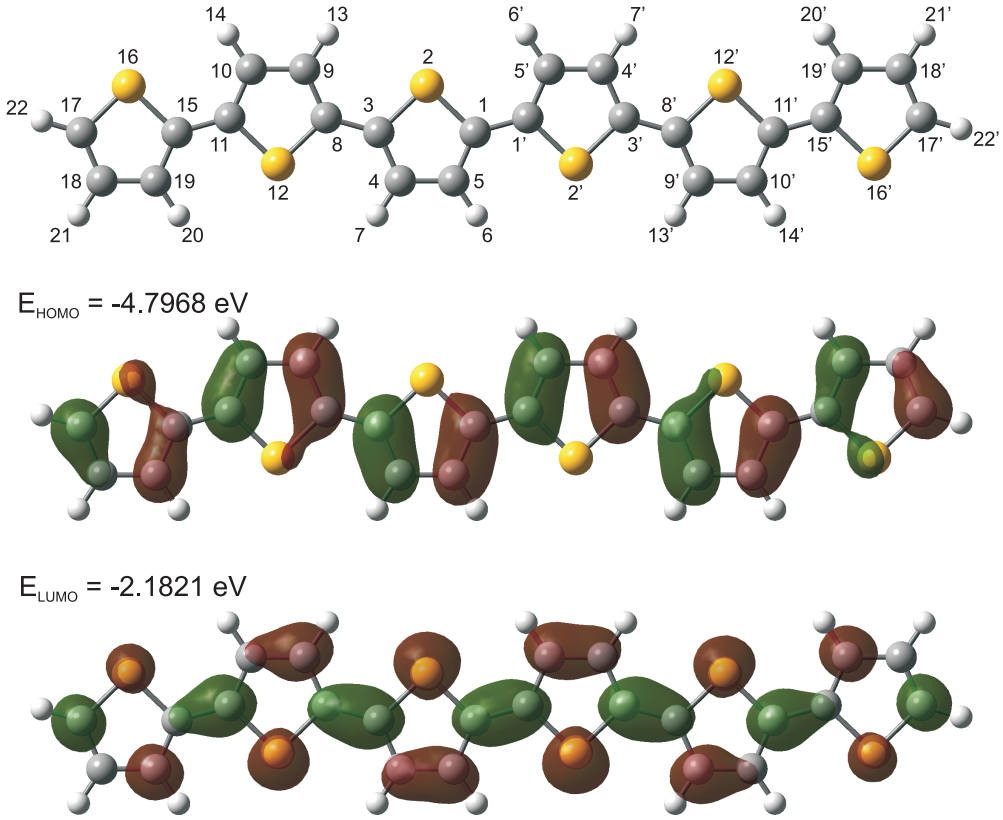

Figure 3.1. Numbering scheme and HOMO-LUMO orbitals for hexathiophene obtained with the PBE functional.

The band gap calculated with the B3LYP functional is in asymptotic agreement with data published by other authors [8]-[9] and agrees fairly with the experimental band gap of 2.21 eV reported for hexathiophene by Chung et al. [10].

3.1.1.2 IR and Raman spectra

Our calculations are able to reproduce the experimental vibrational modes and give better results in cases where the natural symmetry of the considered compounds (C_{2h} and C_{2v}) is imposed and conserved.

We present comparatively in Figs. 3.2 our calculated IR and Raman spectra for the oligothiophenes up to the hexamer, as well as for the 11-mer and 12-mer. As in the case of the geometry optimization, the results obtained with the 6-31G(d) basis set provide the closest agreement with

Table 3.1. Representative in and inter-cycle C-C and C-S bond lengths of hexathiophene resulted from experiments [1] and calculated with the B3LYP and PBE exchange-correlation functionals.

	Exp. (Ref. [1])	B3LYP	PBEPBE
	Å	error (%)	error (%)
C1C1'	1.445(9)	-0.4	-0.6
C3C8	1.45(1)-1.46(1)	-1.0	-1.2
C11C15	1.45(1)	-0.40	-0.6
C1S2	1.730(7)-1.731(7)	1.6	1.8
S2C3	1.733(8)-1.739(8)	1.3	1.4
C11S12	1.729(7)-1.733(7)	1.5	1.7
C8S12	1.733(7)-1.742(8)	1.2	1.4
C15S16	1.719(8)-1.726(8)	2.0	2.2
C17S16	1.704(9)-1.711(9)	1.6	1.6
C1C5	1.37(1)-1.38(1)	0.5	1.4
C3C4	1.36(1)	1.5	2.4
C8C9	1.36(1)	1.5	2.4
C10C11	1.38(1)	-0.1	0.8
C15C19	1.38(1)-1.40(1)	-0.8	0.1
C17C18	1.31(1)-1.32(1)	3.9	4.7
C4C5	1.40(1)-1.41(1)	0.6	0.4
C9C10	1.40(1)	0.9	0.8
C18C19	1.41(1)-1.42(1)	0.5	0.5

the experiment, and in the following are exclusively referred to.

We divide conventionally the whole IR and Raman spectral range for the considered polythiophenes into three distinct regions. The first region extends up to 1000 cm^{-1}, is characterized mainly by out-of-plane vibrations, but also by in-plane modes at the blue end, is quite crowded in terms of IR-active vibrations, but only moderately populated with Raman features. The second region ranges between 1000 cm^{-1} and 1400 cm^{-1} and is moderately occupied by IR spectroscopic features, while Raman modes are better represented, especially for the monomer and the large oligomers. The third region spreads up to 1600 cm^{-1} and is well populated both with IR and Raman-active modes, which correspond mostly to in-plane motions.

As general remark emerging from Figs. 3.2 is the fair agreement of our calculations for the three

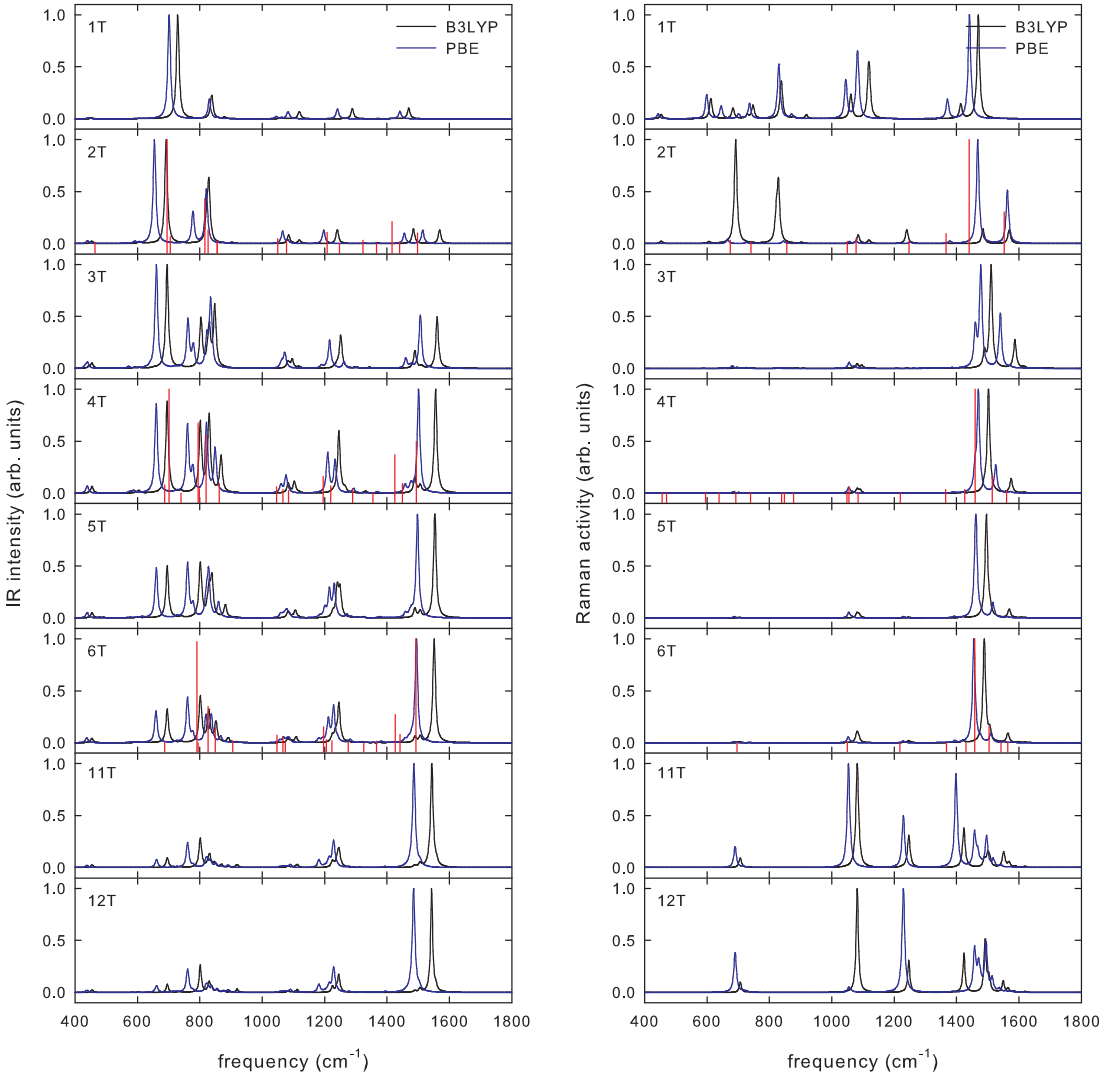

Figure 3.2. IR spectra (left) and Raman spectra (right) for the oligotiophenes obtained with the basis set 6-31G(d) imposing symmetry conservation and experimental peaks with drop lines [1].

smallest even-size oligomers with the available experimental peaks from the literature (represented with vertical drop lines) [1].

The 1400-1600 cm^{-1} region is characterized mainly by in-plane combinations of longitudinal motions of the H atoms with in-ring stretching vibrations of the C=C double bonds.

Two experimental in-plane Raman-active modes occur at 1460 cm^{-1} for the tetramer and at 1458 cm^{-1} for the hexamer [1]. Our PBE calculations reproduce the experimental frequencies with even better accuracy than in the dimer case, namely the relative errors drop to approximately 0.5%

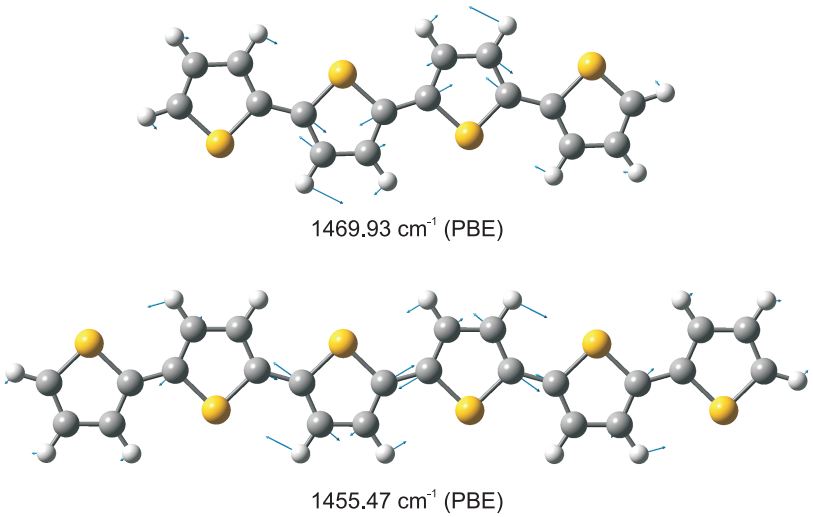

Figure 3.3. In-plane Raman modes of the teramer and hexamer corresponding to the experimental peaks located at 1460 and 1458 cm^{-1} [1], obtained with the PBE functional.

for the tetramer and to 0.1% for the hexamer (see Fig. 3.3). In the case of the hexamer, the peak calculated at 1455.57 cm^{-1} matches fairly the experimental Raman data provided by other groups: Bazzaoui *et al.* at 1455 cm^{-1} [11], Loi *et al.* at 1459 cm^{-1} [12], Weinberg-Wolf *et al.* at 1461 cm^{-1} [13], and Brillante *et al.* at 1460 cm^{-1} [14].

For the frequency range beyond 1600 cm^{-1}, the Raman spectra appear similar for all three even-sized oligomers and are dominated by two strong in-plane modes. The best agreement with the experiments is provided again by the PBE functional. For the tetramer and hexamer, the higher intensity peak is found at slightly higher frequencies (by less than 0.7%) than the experimental ones (see Fig. 3.3).

A technical aspect which needs to be stressed again, this time in connection with the IR and Raman vibrations of the oligomers up to the dodecamer, is that above 1000 cm^{-1} the PBE functional performs consistently more realistically than B3LYP, continuing the trends which have been already established up to hexamer. Overall, from the PBE-based calculations the IR spectra result slightly red shifted and the Raman spectra marginally blue shifted (see Figs. 3.2).

3.1.2 Vibrations of thiophene-fullerene dyads

The following analysis focuses on thiophene-based dyads. In such dyads, the donor and acceptor entities are covalently bonded and several of the coordinates which characterize their relative positions and need to be considered when they are non-bonded are thus eliminated.

3.1.2.1 Infrared-active vibrations

At a first glance, all spectra resemble, excluding, however, a section positioned in the lower frequency range, where most vibrational modes are a result of the thiophene chain vibration. This spectral range extends from 400 to 900 cm^{-1}. The next distinct spectral region with pronounced infrared activity: is situated around 1000-1500 cm^{-1} and is mainly due to fullerene vibrations.

The first region is filled mainly with modes corresponding to carbon-sulphur stretching in the thiophene cycles and some out-of-plane vibrations of the carbon and hydrogen groups. The second region is not particularly different between the different compounds.

For the 1-thiophene dyad, our PBE calculations shows a feature situated at 676 cm^{-1} and corresponds to the vibration caused by the C-H out-of-plane vibrations and was observed experimentally at 700 cm^{-1} by Lewandowska et al [15]. In the spectrum of the 2-thiophene dyad, two bands have been reported in [16]: the first at 724 cm^{-1} and the second, a triplet, was found to peak at 769, 785, and 792 cm^{-1}. These bands are characteristic for C-S in-plane and C-H out-of-plane motions and have been fairly well reproduced by our calculations at 733, for the first band, and at 773 and 783 cm^{-1} for the triplet. In the infrared absorption spectrum of the 4-thiophene dyad we can recognize several of the features which have been experimentally measured for the 1, 2, and 3-thiophene dyads.

In the spectrum of the 5-thiophene dyad, the first calculated vibrational feature is observed at 665 cm^{-1} and is due to out-of-plane C-H vibrations in the terminal thiophene cycle. The same mode was observed experimentally and reported in [16, 15]. The first infrared vibrational mode of the 6-thiophene dyad is located at 665 cm^{-1} and is due to out-of-plane C-H motions activated in the terminal thiophene cycle. The obtained result is in a good agreement with the data reported in. [16].

All studied oligomers show two distinct bands at higher frequencies: one around 2900 cm^{-1}, stemming from CH_3 stretchings in the N-methylglycine part, and another at 3200 cm^{-1}, caused by the in-plane CH stretchings in the thiophene chain part (Fig. 3.4).

For all molecular compounds considered, the above vibrational modes remain active in the trans configuration, as well. Overall, the PBE functional reproduces much better the experimentally measured data without appling any scaling procedures. The spectra generated using the B3LYP functional follow the PBE results, however with a shift towards higher frequencies. Like in the case of isolated thiophene chains, we observe an increase in spectral intensity with increasing molecular size [17].

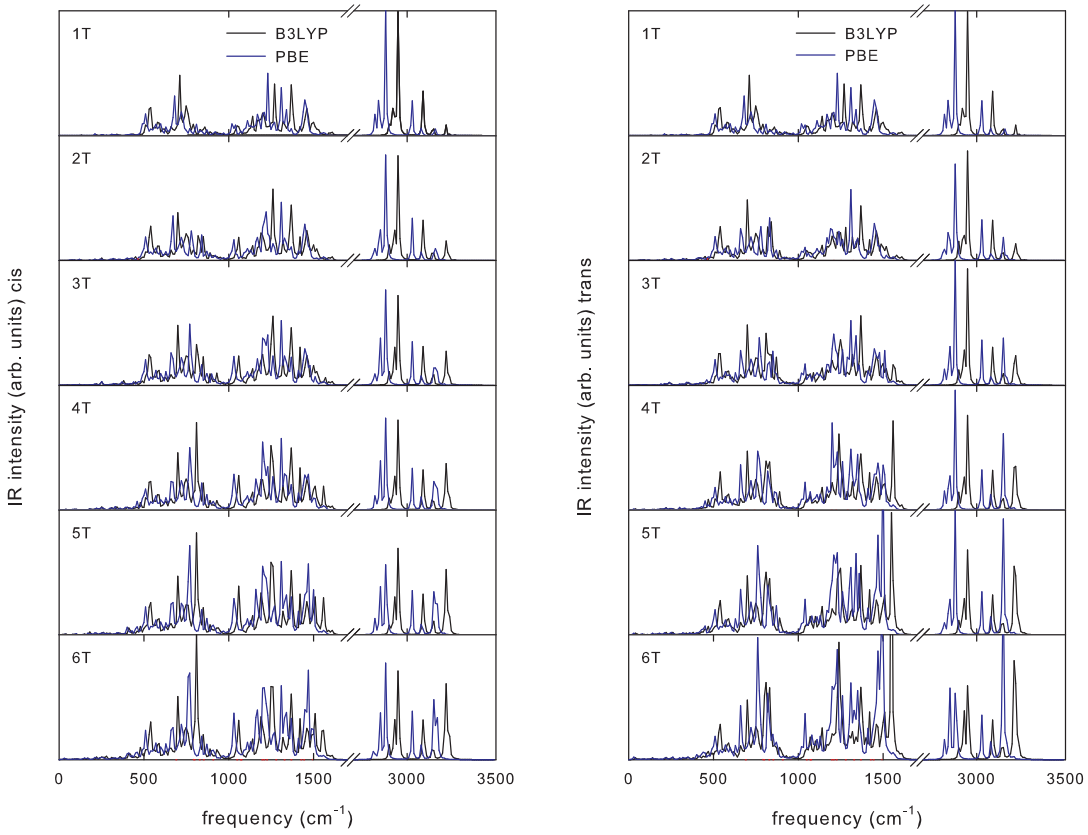

Figure 3.4. IR spectra of cis (left) and trans (right) 1-6 thiophene dyads obtained with the B3LYP (black) and PBE functionals (blue).

3.1.2.2 Raman-active vibrations

The analysis of the Raman spectra is performed in a similar manner with the one for the infrared-active vibrations.remarkably, there are only few noticeable differences between the Raman spectra from small to large molecular systems. The same findings have been also reported in [16].

There are only few spectral regions showing distinctive features with increasing system size. The most important frequency domain ranges between 1400 and 1600 cm^{-1} and this region contains the most intense peaks, which are determined mainly by C=C bond stretching vibrations.

In the experimental spectrum of the 1-thiophene dyad [16], the important features were found in the range between 1000-1600 cm^{-1}. The most representative bands are very well reproduced by our PBE based calculations. In the spectrum of 2-thiophene dyad, the experimental vibrational features were obtained in [16] at the same frequencies as in the case of 1-thiophene dyad. Our PBE calculations were able to reproduce the experimental modes rather accurately. The Raman

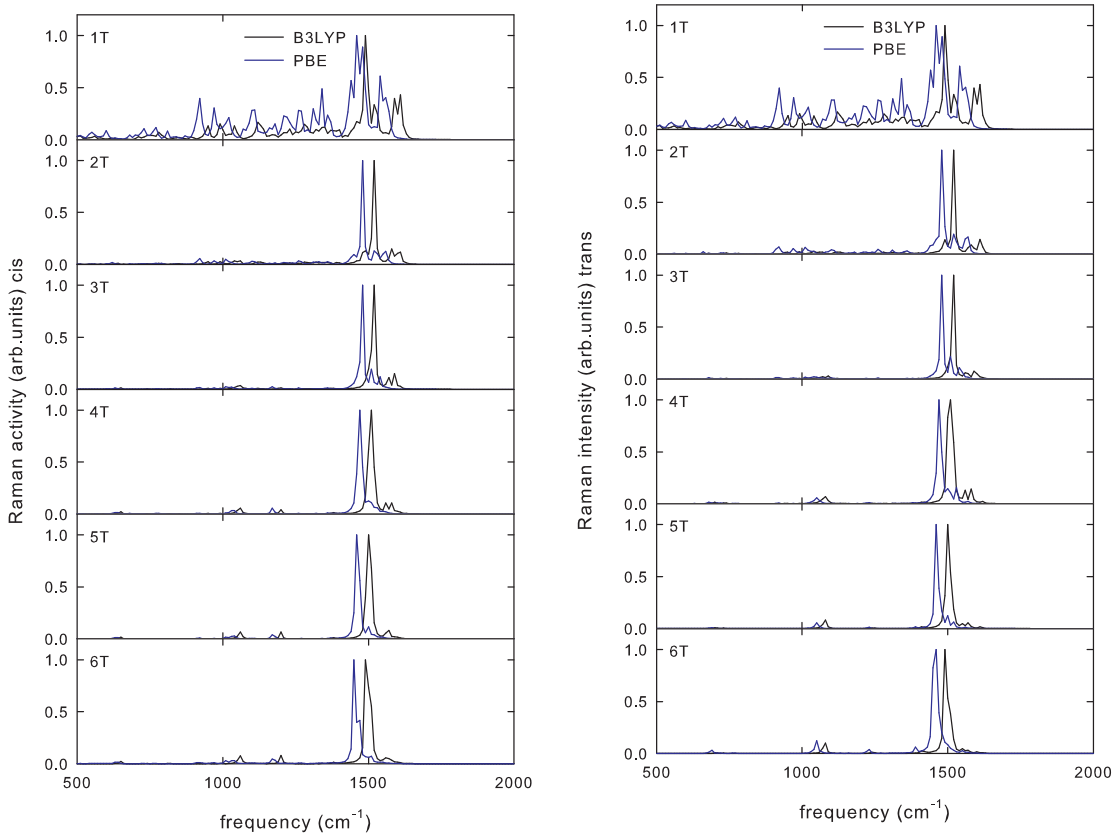

Figure 3.5. Raman spectra of cis (left) and trans (right) 1-6 thiophene dyads obtained with the B3LYP (black) and PBE functionals (blue).

spectrum of 3-thiophene dyad looks little different than for the previous ones. The main feature was measured in [16] at 1459 cm^{-1} and was calculated by us at 1478 cm^{-1}.

The spectrum of the next three dyads are very similar with some minor exceptions. The first spectral feature was calculated for the 4 and the 5-thiophene dyads at 1033 cm^{-1} and it describes the C-C-H vibrations. For the largest intensity mode there are noticeable differences in the spectra of the last three dyads. This mode is mainly due to C=C in-plane stretchings and is situated at 1473 cm^{-1} for the 4-thiophene dyad and is also visible in infrared. For the 5 and 6-thiophene dyads the Raman spectra exhibit the last feature at 1458 cm^{-1} (which coincides to the one experimentally measured in [16] for 1, 2, and 3-thiophene-dyads), and at 1452 cm^{-1}, respectively.

As in the infrared spectra, the trans version of the above studied molecules presents the same vibration modes with a slight shift towards smaller frequencies, Figure. 3.5 right. Also, in this case the PBE reproduces significantly better the previous published experimental data than B3LYP.

3.2 Molecular dynamics simulations of 3-thiophene-based dyads

There is still another beneficial feature of the thiophene-based dyads, which is yet neither fully understood, nor efficiently used to its fullest potential, namely their capacity of self-arrangement when fabricated as thin films.

Specifically, we have studied the 3-thiophene-based dyad P3HT-(C_{60}N), which stands out by its electronic properties, namely a bandgap which is lower as compared to other compounds, reason why is suitable for photovoltaic applications. On the existence of the covalent bond between the donor and acceptor rests the main advantage of such dyads of being able to form structured films.

Being by nature a dynamic process, we have investigated the self-assembling of the thiophene-based dyads by Molecular Dynamics (MD) simulations. To this end, we have employed the AMBER 12 package [27]. The simulated system was typically constructed of 216 dyads (each composed, in turn, of 92 atoms). The total of 19872 atoms have been enclosed in a simulation box of dimensions $6.38 \times 6.08 \times 6.37$ Å and periodic boundary conditions have been applied in all three Cartesian directions.

A subsequent equilibration of roughly 1 ns completed the preparation of the initial configuration. Both at room temperature (300K) and the higher temperature considered (1300K), the data collection time from the production runs extended over as long as 10 ns. One should note, that performing NVT simulations (with constant number of particles, volume and temperature) one employs actually the kinetic definition of the temperature, which does not perfectly match the physical definition. The main measured quantities, defined as time-averages along the MD trajectories, used to characterize dynamically the evolution of the system morphology and dyad mobility have been the radial distribution function and the diffusion coefficient, respectively.

The observed radial distribution functions for the pairs C_{60}-C_{60} and C_{60}-thiophene are plotted respectively in Figs. 3.6-3.7. Overall, the distributions show the typical behavior, with an asymptotic value of 1, implying that under any particular direction a generic moiety would have at least one counterpart. However, as regards the structured peaks at finite inter-distances, there are significant differences.

As can be seen from the left panel of Fig. 3.6, where the RDF for the C_{60}-C_{60} pair at room temperature is depicted, the most probable is a complex composed of six 3-thiophene dyads, which surround the generic central dyad at an average distance of about 9.8Å. In counting the nearest neighbors, instead of barely considering the magnitude of the major peak, we have considered its integral.The more remote spherical vicinity of any dyad can be seen to be structured, the RDF

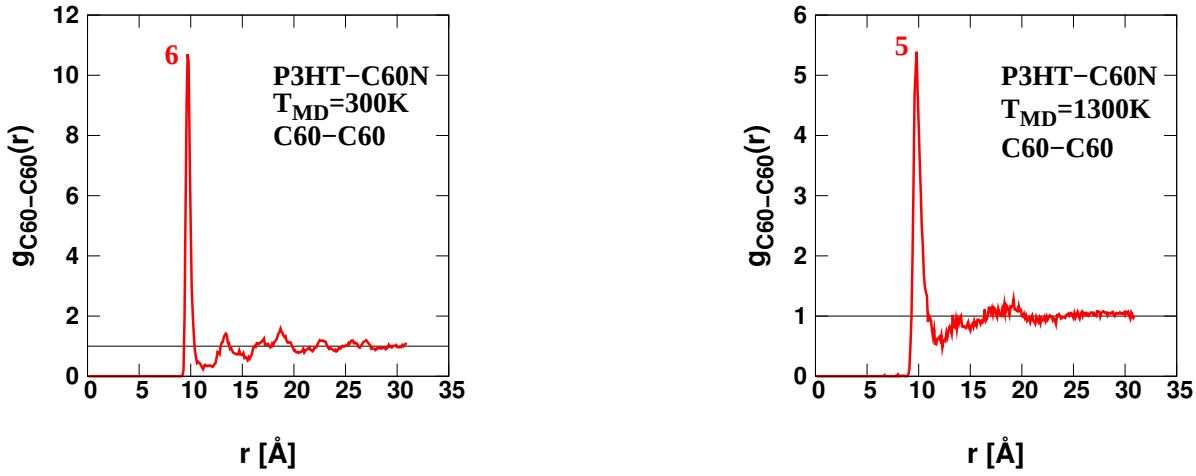

Figure 3.6. Radial distribution functions for the C_{60}-C_{60} moieties in the P3HT-(C_{60}N) system at 300K (left) and 1300K (right).

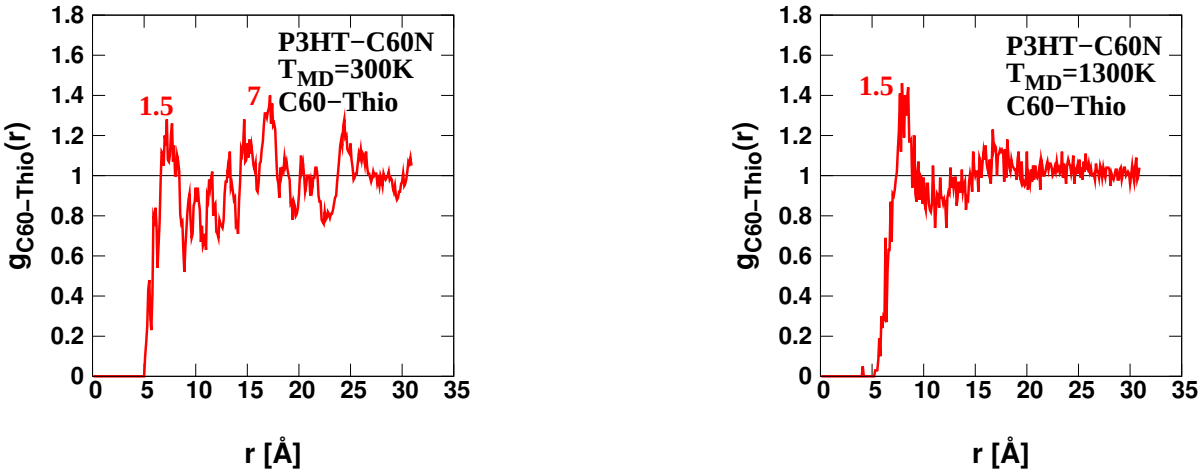

Figure 3.7. Radial distribution functions for the C_{60}-thiophene moieties in the P3HT-(C_{60}N) system at 300K (left) and 1300K (right).

evidencing further peaks around 13, 16.5 and 18 Å.

At the higher temperature (1300K), the C_{60}-C_{60} radial distribution function (see the right panel of Fig. 3.6) maintains the general features found at room temperature. However, as evidenced by the integral of the main peak, the coordination reduces from 6 to 5 and the secondary peaks become more diffuse, indicating, as expected, a less structured vicinity.

The C_{60}-thiophene radial distribution functions (see Figs. 3.7), complement the information

provided by the C_{60}-C_{60} RDFs, indicating also some orientation ordering within the system of dyads. A first sphere of coordination is identified around 7.5 Å at 300K and, slightly shifted to about 8 Å at 1300K, both evidencing on average 1.5 thiophene chains around any $C_{60}N$ moiety. Having in view the most probable C_{60}-C_{60} distance of 9.8 Å, it becomes obvious that head-to-head relative positions of two neighboring dyads are highly improbable. Nevertheless, in general, the orientation ordering is much less pronounced than the C_{60}-C_{60} positional one.

A second C_{60}-thiophene coordination sphere can be identified at room temperature at about 17.3 Å from any $C_{60}N$ derivative and it results on average from the presence of 7 thiophene chains (left panel of Fig. 3.7). At high temperature (right panel of Fig. 3.7), the average radial C_{60}-thiophene structuring becomes washed-out, as in the case of the C_{60}-C_{60} RDF, however, with a broad coordination sphere still recognizable around 18 Å.

The thiophene-thiophene RDF for 300K, shows a discrete radial probability maximum around 7 Å, involving on average 0.5 thiophene chains, and yet a second one at about 12 Å, involving 3 chains around any thiophene chain. This anyway rather vague structuring almost vanishes at the higher temperature. Obviously, there are only marginal orientation correlations between the thiophene chains.

As mentioned in chapter 2, for large evolution times of the system as compared to the characteristic collision interval of the system, the self-diffusion coefficients can be calculated according to the Einstein expression:

$$D = \lim_{t\to\infty} \frac{1}{6Nt} \left\langle \sum_{i=1}^{N} \left[\mathbf{r}_i\left(t\right) - \mathbf{r}_i\left(0\right)\right]^2 \right\rangle, \tag{3.1}$$

and, essentially, it is proportional to the mean square displacements of the particle positions with respect to their initial positions divided by the simulation time.

The mean square displacements (MSDs) of the thiophene-fullerene dyads for the temperatures 300K and 1300K, along with the corresponding self-diffusion coefficients D are plotted respectively in Figs. 3.8 and 3.9. As one can easily notice, there is a qualitative difference between the profiles at low and high temperatures.

A most significant finding is that the MSDs at 300K are three orders of magnitude lower than at 1300K, corresponding to net displacements as low as 2 Å/ns. In addition the MSD profile at 300K is very noisy (left panel of Fig. 3.8) and, instead of behaving quasi-linearly in the limit $t \to \infty$, it saturates, indicating the degradation of the spatial correlations between the dyads.

At high temperatures, the quasi-linear time-dependence of the MSD is apparent from the left

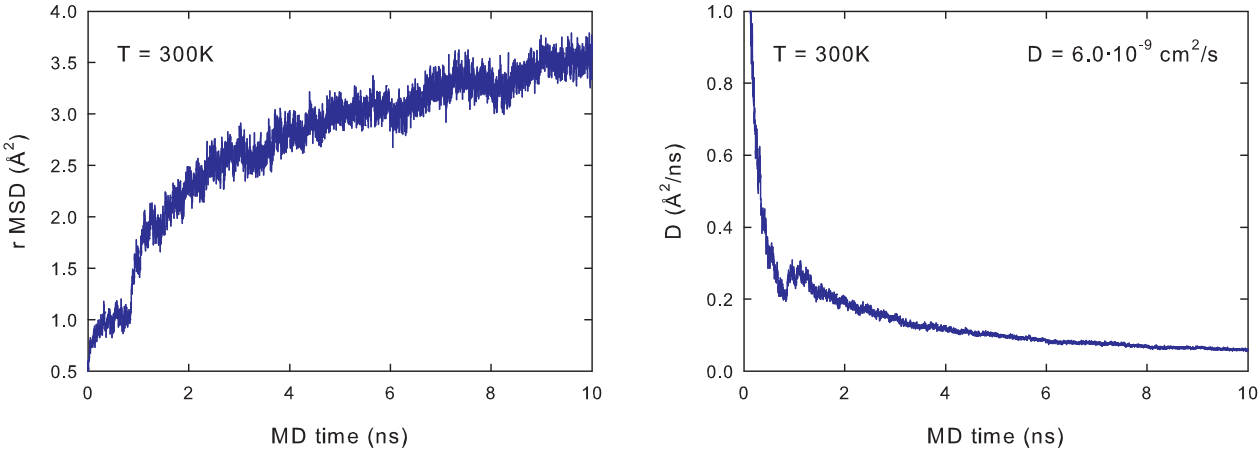

Figure 3.8. Mean Squared Displacement and self-diffusion coefficient for the P3HT-(C_{60}N) dyad at 300K.

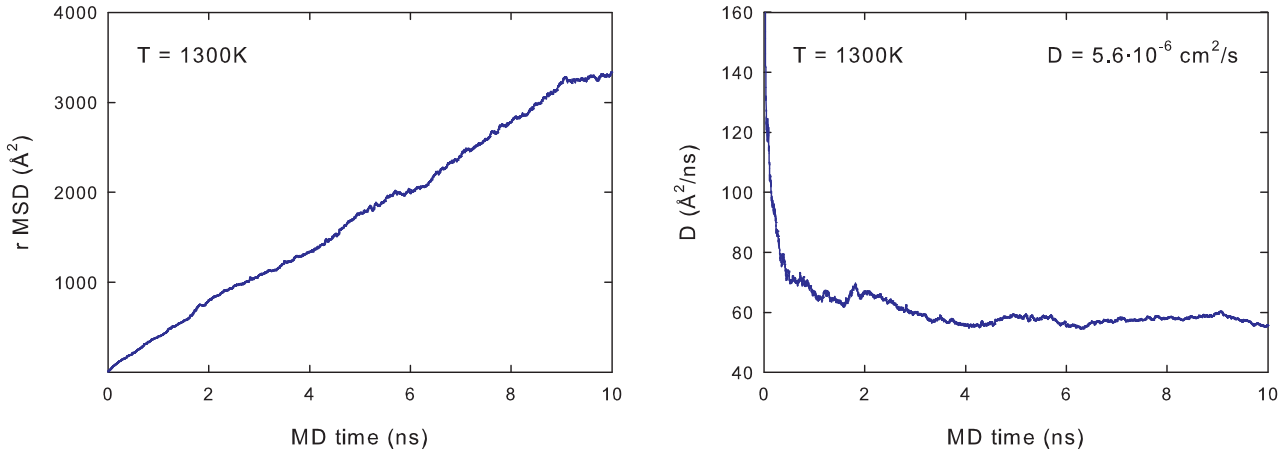

Figure 3.9. Mean Squared Displacement and self-diffusion coefficient for the P3HT-(C_{60}N) dyad at 300K.

panel of Fig. 3.9, and it is obviously affected by significantly less noise than at low temperature. The corresponding diffusion coefficient (right panel) turns out to be three orders of magnitude larger than at 300K and amounts to a physically reasonable value of 5.6×10^{-6}cm^2/s.

One of the major findings of the MD simulations on the P3HT-(C_{60}N) dyads, with direct practical implications is that an efficient self-assembling of a thin dyad film cannot be achieved at room temperature, where the reorientation of the dyads is hampered and one cannot really speak of diffusion. Only at high MD temperatures one can actually find a genuine diffusion process, which can bring about the self-organization of the dyads by annealing.

4

Charge transfer in fullerene-based bulk heterojunctions

4.1 Electron dynamics in donor-acceptor systems

Due of their different architecture as compared to the double layer structures, the bulk heterojunctions (BHJ) show an increased charge transfer between the donor-acceptor molecules since the excitons are created throughout in the bulk.

In the reported study, we have investigated computationally the electron transfer between donor-acceptor molecules involving two different donor categories, namely chain and star-shaped. Both of these types of donor molecules can be mixed individually with fullerene derivatives (playing the role of acceptor parts) to form bulk heterojunction active layers.

4.2 Electron dynamics formalism

For the calculation of the electron transfer (ET) in our systems we basically used the quantum mechanical (QM) methodology developed in the group of Professor Francesco Zerbetto, from the Department of Chemistry "Ciamician" at the University of Bologna [18, 19, 20].

The method is based on the quantum mechanical description of the electron dynamics in the formalism of Roothaan's equation and using for the temporal evolution Cayley's algorithm. Our improved version of this method, which identifies the main computational bottlenecks was recently published in [21]. Moreover, the computational speed was increased by 50 times using the new graphic processing unit (GPU) as compared to the classical CPU's.

The time-dependent Schroedinger equation [22] is solved via Cayley's algorithm [18]:

$$\Phi_j\left(\mathbf{r}, t+\Delta t\right) = \left(\mathbf{I} + \frac{i\Delta t}{2\hbar}\mathbf{H}'\right)^{-1}\left(\mathbf{I} - \frac{i\Delta t}{2\hbar}\mathbf{H}'\right)\Phi_j\left(r, t\right), \tag{4.1}$$

where Φ_j is the one electron molecular orbital (MO) of a multi-electron system, $\mathbf{H}'$ is the corresponding Hamiltonian operator in matrix form, Δt an incremental time step, t is the time coordinate, $\hbar$ is the Dirac constant, and i is the imaginary unit. The QM description in the Hamiltonian is at some level of theory (HF, DFT, CCSD(T), MCSCF, CI, etc) and MOs are expressed as linear combinations of a chosen set of basis functions (most commonly atom-centered Cartesian Gaussians), that is the LCAO approach [23]. As the Hamiltonian from the above equation represents a matrix, the expressions $1+$, $1-$, and $()^{-1}$ also refer to matrix syntax.

The Cayley algorithm provides a step-by-step solution with respect to the time coordinate, so that by successive forward propagation in time, a complete image of the time dependence can be established.

4.3 Chain-type oligothiophenes

In previous publications, Blouin et al. [24] reported the synthesis and performance of a PCDTBT-based device accounting for 3.6% power conversion efficiency from a BHJ-type structure with a V_{OC} value of nearly 0.9V. Later Park et al. [25] reported an efficieny of 6.1 % for the PCDTBT/[6,6]-phenyl C_{71} butyric acid methyl ester ($PC_{71}BM$) device, which is one of the best performances among any other BHJ-based systems studied at present.

Our computational studies are focused on the above mentioned system, PCDTBT [24], as donor molecule and [6,6]-phenyl C_{71} butyric acid methyl ester ($PC_{71}BM$) [26] as acceptor counterpart.

In our study, we employ two variants of initial preparation of the system. In the first case we calculate the donor population transfer for optimized relative geometries using the GAUSSIAN package [3], while in the second case we perform the same type of calculations using a snapshot extracted from molecular dynamics simulations carried out with AMBER12 package [27].

The distance between the donor/acceptor was optimized in sequence using two different functionals B3LYP [4] and PBE [5]. In both cases the donor-acceptor distance was almost invariant (3.4 Å). The total population transfer amounts to about 60% and, as expected, we have not observed significant differences between the results obtained when using different functionals.

Figure 4.1 plots the evolution of the LUMO orbitals involved in the electronic transfer for the optimized system. As can be seen, the primary orbitals involved in the transfer are LUMO and

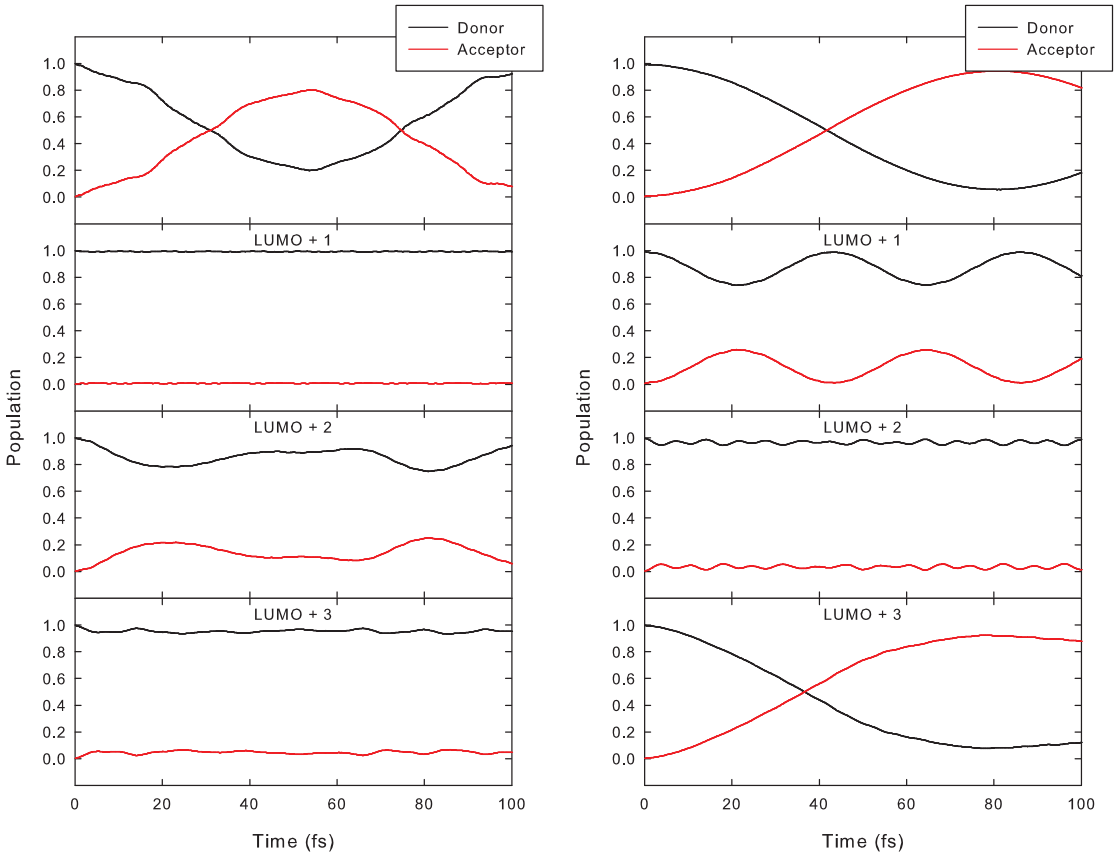

Figure 4.1. Electron transfer for the PCDTBT/PC70BM system optimized by DFT (left) and extracted from an MD snapshot (right).

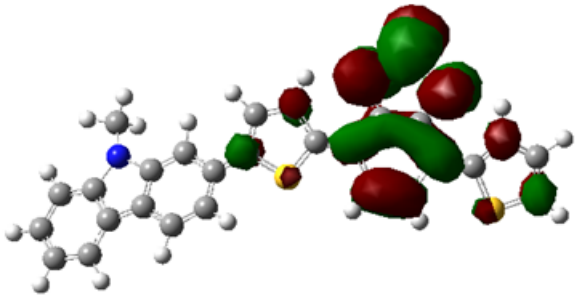

Figure 4.2. LUMO orbital for the PCDTBT/PC70BM configuration.

LUMO+2, with a population transfer of 43% and 13%, respectively. The population transfer from the LUMO orbital takes place over a period of 100 fs within the calculated range.

The molecular dynamics snapshot used in our study was chosen from a distribution of several geometries of the system simulated at room temperature. As part of the methodology of using MD

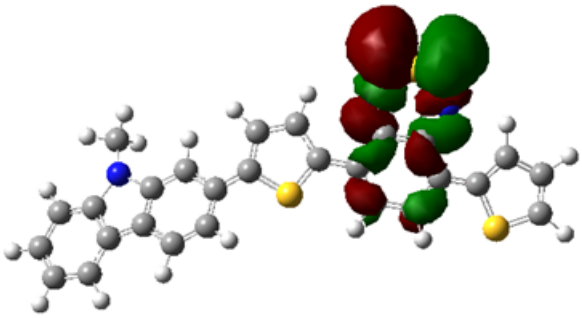

Figure 4.3. LUMO+3 orbital for the PCDTBT/PC70BM configuration extracted from an MD snapshot.

snapshots, we have also perform the analysis using the data generated during the first 100 fs of simulation. The detailed electronic transfer which occurs for each orbital is shown in Fig. 4.1 right. The approximate calculated value of the total population transfer of this system is almost double as compared to the case where the relative distance between the donor/acceptor pair was optimized. The primary orbitals involved in the transfer are LUMO (Fig. 4.2) and LUMO+3 (Fig. 4.3), respectively. In the case of the LUMO orbital a transfer of 56% occured and for LUMO+3, a value of 61% was obtained.

In conclusion, the total population transfer in the two analyzed situations is rather different, both quantitatively and qualitatively. In both cases two orbitals play a major role, one being the LUMO orbital. However, by case, in the flatter optimized structure, the LUMO+2 plays the second most significant role, while, in the MD simulated structure, the LUMO+3 has significant contributions.

4.4 Star-shape oligothiophenes

The second type of investigated thiophenes-based donor molecules is characterized by a star–like shape. These particular oligomers attract a lot of attention because they exhibit many interesting properties, like self-assembly characteristics, which can be applied to forming new molecular structures.

In our transport calculations we have considered the trithienobenzene core in two distinct configurations: trans and cis (Figs. 4.4), described in detail in [28]. We have built the donor/acceptor molecular systems by bringing the planar molecule (donor) in the proximity of the fullerene (acceptor) in such way that the benzene cycle from the donor molecule is parallel with and overlaps a hexagon of the fullerene.

The optimizations performed with the two exchange-correlation functionals (B3LYP and PBE)

Figure 4.4. Structures of trithiophene trans (left) and cis (right)

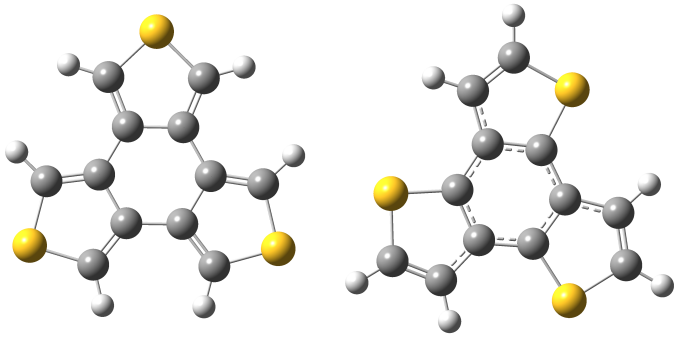

reveal that the relative positions of the donor and acceptor molecules slightly depend on the used functional (Table 4.1), with the donor-acceptor center-to-center distances obtained with the B3LYP functional typically exceeding the values yielded by using the PBE functional. As expected, the small but genuine differences in the geometrical configurations are reflected by corresponding differences in the donor-acceptor population transfer.

In conclusion, whereas the trithiophene compound in trans configuration shows a tendency of increasing the electron transfer between the donor and acceptor moieties with the decrease of the relative distance between the donor-acceptor pair, in the case of the cis configuration, the electron transfer decreases with decreasing distance.

Overall, the molecular compound in cis configuration features a significantly enhanced donor-acceptor electron transfer as compared to the trans configuration. The rather moderate population transfer for the trans system is to be ascribed to all four lowest LUMO orbitals (LUMO, LUMO+1, LUMO+2, and LUMO+3), while in the case of the cis configuration, for the one order of magnitude stronger electron transfer mainly the LUMO and LUMO+1 orbitals are responsible.

Pursuing the idea that the relative distance between the donor and acceptor affects in a decisive manner the population transfer, we chose the trans configuration to perform a study aimed to

Table 4.1. Relative donor-acceptor distance and average population transfer for trithiophene (cis and trans) optimized with the B3LYP and PBE functionals

Donor type	Functional	Relative distance [Å]	Population transfer [%]
Trithiophene-trans	B3LYP	3.9	7.7
Trithiophene-trans	PBE	3.7	9.6
Trithiophene-cis	B3LYP	4.1	11.38
Trithiophene-cis	PBE	3.8	11.11

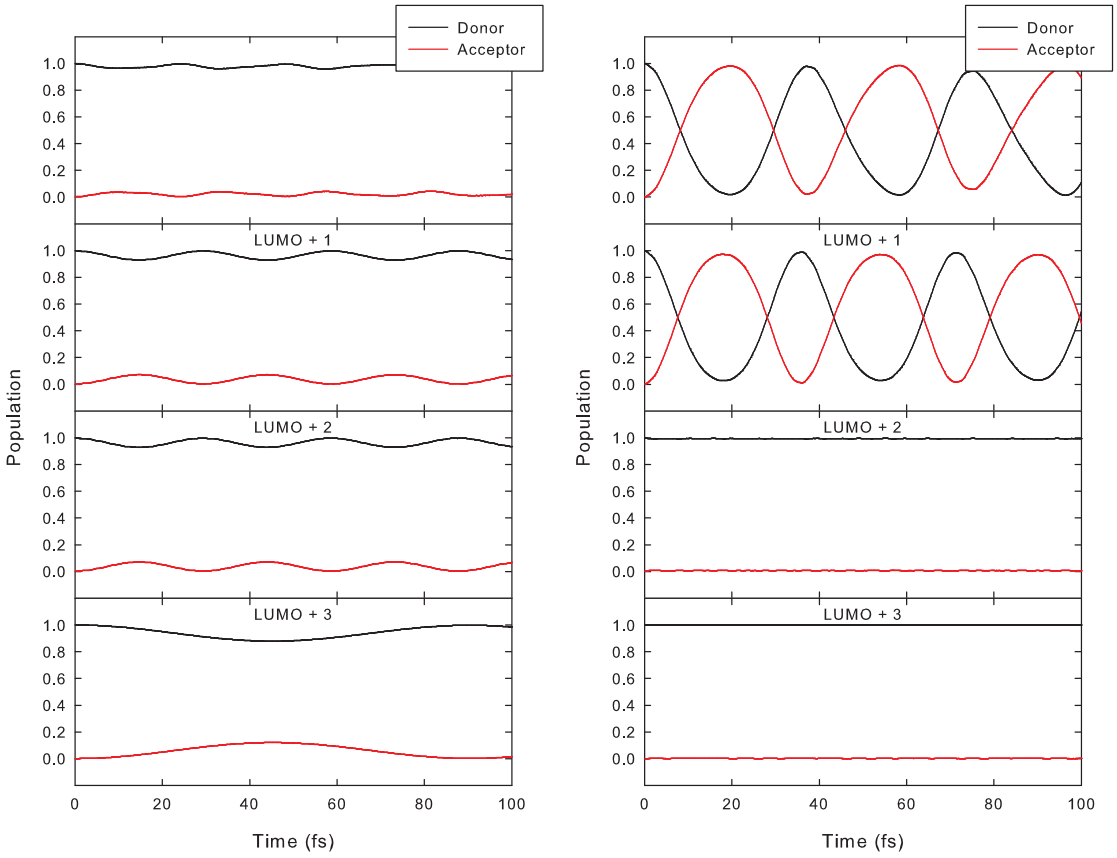

Figure 4.5. Donor-acceptor population transfer in trithiophene trans (left) and cis (right) from the LUMO, LUMO+1,LUMO+2, and LUMO+3 electronic levels.

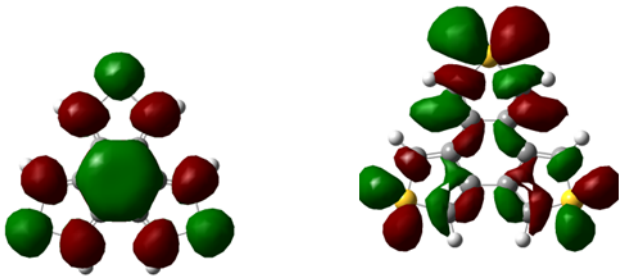

Figure 4.6. LUMO (left) and LUMO+3 (right) orbitals for trithiophene trans, showing the maximum electron transfer.

estimate the donor-acceptor distance corresponding to the optimal electron transfer.

In conclusion, the best electronic transfer occurs at a center-to-center donor-acceptor distance of 3.4 Å. The strongest localized contribution to the population transfer occurs for the LUMO orbital

Figure 4.7. LUMO+1 (left) and LUMO+2 (right) orbitals of trithiophene trans.

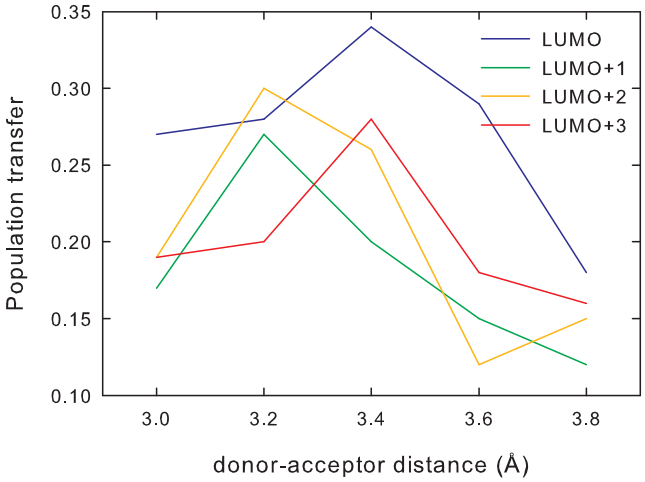

Figure 4.8. Population transfer vs. intermolecular distance

of the donor (Fig. 4.6, left) when the thiophene ring is facing one of the six-membered rings of the fullerene. Similar findings have been reported by Tamura et al. [29]. The higher orbitals, LUMO+1 and LUMO+2, show evenly distributed electron densities across the donor molecules (Fig. 4.7).

An interesting behavior was found at donor-acceptor distances below 3.4 Å, namely the activity of LUMO+1 and LUMO+2 is increasing rapidly up to 3.2 Å and then it decreases all the way to the end of the simulated time interval. The activity of the LUMO and LUMO+3 orbitals is increasing gradually up to a donor-acceptor distance of 3.4 Å, then it is decreasing similarly with the other two orbitals (Fig. 4.8).

5
Conclusions

5.1 Morphology

The thesis reports on DFT computational investigations of the IR and Raman-active vibrations of polythiophenes with up to 12 cycles and matches the results against experimental evidence from the literature.

As a general remark concerning the equilibrium structures of the oligothiophenes, the C-C distances between in-ring atoms are consistently better reproduced by the PBE functional but, on the other hand, the inter-ring C-C and in-ring C-S bond lengths are better reproduced by the B3LYP functional. The bandgaps calculated for the 12 considered thiophenes show a monotonic decreasing trend with increasing chain size and for the B3LYP functional they converge towards the hexathiophene bandgap resulting from the measurements.

Regarding the IR and Raman vibrations of tyhe polythiophenes, it is worth noting that we achieved with both functionals an agreement with the experiments which is superior to previous reports, even without applying any frequency scaling. The B3LYP functional produces better agreement with the experiments mainly in the lower frequency range (below 1000 cm^{-1}), in particular in describing the out-of-plane modes which are predominant in this domain and on the other hand, the PBE functional performs significantly better in the intermediate and higher frequency domain (above 1000 cm^{-1}), where the frequencies predicted for the prevailing in-plane vibrations match remarkably the experimental values.

For the second class of molecular systems investigated in the thesis in terms of structural and

vibrational properties, namly thiophene-fullerene dyads, both the IR and Raman features are better reproduced with the PBE functional and are definitely superior as concerns the agreement with the experiments than previously published calculations.

5.2 Charge transfer

The total population transfer for the system containing a chain-type donor is higher in the snapshot extracted from MD simulations than in the optimized case having a particular geometry that favors the transfer from donor to acceptor. In both configurations the LUMO orbital plays the major role and by case, in the more flat optimized structure, LUMO+2 plays a bigger role and in the MD simulated structure, the LUMO+3 has a bigger contribution.

The relative distance for the optimized star-type donor based system does not change significantly with the configuration type (cis/trans). On the other hand, the electron transfer is very different between the cis and trans configurations. The systems implying donors in cis configuration show a better electron transfer than the trans-based system, amounting to an average of 54%. In the cis configuration, only the LUMO and LUMO+1 orbitals are involved, while for the trans system, the population transfer is distributed over all four monitored orbitals (LUMO, LUMO+1, LUMO+2, and LUMO+3).

Pursuing the idea that the relative distance between the donor and acceptor affects in a decisive manner the population transfer, we chose the trans configuration to perform a study aimed to estimate the donor-acceptor distance corresponding to the optimal electron transfer. The best electronic transfer was found to occur at a center-to-center donor-acceptor distance of 3.4 Å. Responsible for the strongest localized contribution to the population transfer is the LUMO orbital of the donor when the thiophene ring is facing one of the six-membered rings of the fullerene.

5.3 Outlook

As future steps of this research, we will consider further donor-acceptor combinations susceptible of high efficiency electron transfer, from among the ones mentioned in chapter 4, but which have not been analyzed yet as part of the reported investigations. One of the most promising donor candidates is anticipated to be PCPDTBT (poly[2,6-(4,4-bis-alkyl-4H-cyclopenta[2,1-b;3,4-b]dithiophene)-alt-4,7-(2,1,3-benzothiadiazole)]) and a matching acceptor would be $PC_{70}BM$ ([6,6]-phenyl C70-butyric acid methyl ester). Several such donor-acceptor pairs will be investigated in detail.

The theoretical methodology will be similar to the one validated in this thesis and will imply: (1) DFT-based geometry optimizations using comparatively different exchange-correlation functionals; (2) molecular dynamics simulation of morphology evolution during the film growth; (3) electron transfer calculations based on the quantum mechanical formalism developed, using either optimized structures or MD snapshots.

The systems showing the best potential for electron transfer will be subject to extensive MD simulations under various conditions, in a wide range of temperatures. Based on the analysis of the resulted radial distribution functions, the most representative configurations will be extracted and will be employed in electron dynamics calculations of population transfer and, finally, compared with the charge transfer efficiencies obtained for the optimized structures.

With a view to providing ”rules-of-thumb” for practical fabrication of structured organic thin films based on bulk heterojunctions, the study will also focus on optimizing the relative donor-acceptor positions for significant population transfer.

The detailed investigations of the charge transfer in the representative geometrical arrangements chosen for the considered donor-acceptor pairs will provide ”performance maps”, which, by averaging, will enable the calculation of charge carrier mobilities in more realistic extended systems, as models for real bulk heterojunction-based materials. Equally, the calculations are expected to offer information about the nature of the organic donor-acceptor type semiconducting molecules which are most suitable for building self-arranged structures.

References

[1] A. Degli Esposti, O. Moze, C. Taliani,J. T. Tomkinson, R. Zamboni, and F. Zerbetto, The intramolecular vibrations of prototypical polythiophenes, J. Chem. Phys. 104 (1996) 9704-9718.

[2] A. Degli Esposti, M. Fanti, M. Muccini, C. Taliani, and G. Ruani, The polarized infrared and Raman spectra of a-T6 single crystal: An experimental and theoretical study, J. Chem. Phys. 112 (2000) 5957-5969.

[3] M. J. Frisch, G. W. Trucks, H. B. Schlegel, G. E. Scuseria, M. A. Robb, J. R. Cheeseman, J. A. Montgomery, Jr., T. Vreven, K. N. Kudin, J. C. Burant, J. M. Millam, S. S. Iyengar, J. Tomasi, V. Barone, B. Mennucci, M. Cossi, G. Scalmani, N. Rega, G. A. Petersson, H. Nakatsuji, M. Hada, M. Ehara, K. Toyota, R. Fukuda, J. Hasegawa, M. Ishida, T. Nakajima,

Y. Honda, O. Kitao, H. Nakai, M. Klene, X. Li, J. E. Knox, H. P. Hratchian, J. B. Cross, C. Adamo, J. Jaramillo, R. Gomperts, R. E. Stratmann, O. Yazyev, A. J. Austin, R. Cammi, C. Pomelli, J. W. Ochterski, P. Y. Ayala, K. Morokuma, G. A. Voth, P. Salvador, J. J. Dannenberg, V. G. Zakrzewski, S. Dapprich, A. D. Daniels, M. C. Strain, O. Farkas, D. K. Malick, A. D. Rabuck, K. Raghavachari, J. B. Foresman, J. V. Ortiz, Q. Cui, A. G. Baboul, S. Clifford, J. Cioslowski, B. B. Stefanov, G. Liu, A. Liashenko, P. Piskorz, I. Komaromi, R. L. Martin, D. J. Fox, T. Keith, M. A. Al-Laham, C. Y. Peng, A. Nanayakkara, M. Challacombe, P. M. W. Gill, B. Johnson, W. Chen, M. W. Wong, C. Gonzalez, and J. A. Pople, Gaussian 03, Revision B. 01, Gaussian Inc., Pittsburgh, PA, 2003.

[4] A. D. Becke, J. Chem. Phys. 98, 5648 (1993); C. Lee, W. Yang, and R. G. Parr, Phys. Rev. B 37 (1988) 785-789.

[5] J. P. Perdew, K. Burke, and M. Ernzerhof, Phys. Rev. Lett. 77 (1996) 3865-3868.

[6] G. Horowitz, B. Bachet, A. Yassar, P. Lang, F. Demanze, J.-L. Fave, and F. Garnier, Growth and Characterization of Sexithiophene Single Crystals, Chem. Mat. 7 (1995) 1337-1341.

[7] S. M. Bouzzinea, M. Hamidi, M. Bouachrine, Density Functional Theory Study of Electroactive Materials Based on Thiophene in Their Neutral and Doped States, J. Appl. Chem. Res. 11 (2009) 40-46.

[8] K.-F. Braun and S. W. Hla, Charge transfer in the TCNQ-sexithiophene complex, J. Chem. Phys. 129 (2008) 064707-1-7.

[9] S. Pesant, P. Boulanger, M. Cote, M. Ernzerhof, Ab initio study of ladder-type polymers: Polythiophene and polypyrrole, Chem. Phys. Lett. 450 (2008) 329-334.

[10] T. C. Chung, J. H. Kaufman, A. J. Heeger, F. Wudl, Charge storage in doped poly(thiophene): Optical and electrochemical studies, Phys. Rev. B 30 (1984) 702-710.

[11] E. A. Bazzaoui, G. Levi, S. Aeiyach, J. Aubard, J. P. Marsault, and P. G. Lacaze, SERS Spectra of Polythiophene in Doped and Undoped States, J. Phys. Chem. 99 (1995) 6628-6634.

[12] M. A. Loi, Q. Cai, H. R. Chandrasekhar, M. Chandrasekhar, W. Graupner, G. Bongiovanni, A. Mura, C. Botta, F. Garnier, High pressure study of the intramolecular vibrational modes in sexithiophene single crystals, Synthetic Metals 116 (2001) 321-326.

[13] J.R. Weinberg-Wolf and L.E. McNeil, Resonant Raman spectroscopy on a-hexathiophene single crystals, Phys. Rev. B 69 (2004) 125202-1-4.

[14] A. Brillante, I. Bilotti, C. Albonetti, J.-F. Moulin, P. Stoliar, F. Biscarini, and D. M. de Leeuw, Confocal Raman Spectroscopy of a-Sexithiophene: From Bulk Crystals to Field-Effect Transistors, Adv. Funct. Mater. 17 (2007) 3119-3127.

[15] K. Lewandowska, A. Graja, B. Barszcz, A. Biadasz, and D. Wrobel Raman and infrared studies of molecular orientation in fullerene-thiophene films New J. Chem. 35 (2011) 1291-1295.

[16] B. Barszcz, B. Laskowska, A. Graja, E. Y. Park, T. Kim, and K. Lee Vibrational spectroscopy as a tool for characterization of oligothophene-fullerene linked dyads, Chem. Phys. Lett 479 (2009) 224-228.

[17] S.C. Pop and T.A. Beu, Vibrations of polythiophene, Computational and Theoretical Chemistry 995 (2012) 66-74.

[18] A. Acocella, J. A. Garth, F. Zerbetto, J. Phys. Chem. A 2006, 110, 5164.

[19] J. A. Garth, A. Acocella, F. Zerbetto, J. Phys. Chem. A 2008, 112, 9650.

[20] A. Acocella, J. A. Garth, F. Zerbetto, J. Phys. Chem. B 2010, 114, 4101.

[21] S. Hoefinger, A. Acocella, **S.C. Pop**, T. Narumi, K. Yasuoka, T. Beu, and F. Zerbetto, *GPU-Accelerated Computation of Electron Transfer*, J. Comput. Chem. (2012) 33, 2351-2356.

[22] E. Schroedinger, Ann. Phys.-Leipzing, 79 (1926) 361.

[23] A. Szabo and N. S. Ostlund, *Modern Quantum Chemistry: Introduction to Advanced Electronic Structure Theory*, Dover Publications, Mineola, New York, 1996.

[24] Blouin, N., Michaud, A. Leclerc, M., *A low-bandgap poly(2,7-carbazole) derivative for use in high-performance solar cells*, Adv. Mater. 19, 2295–2300 (2007).

[25] S.H. Park, A. Roy, S. Beaupre, S. Cho, N. Coates, J.S. Moon, D. Moses, M. Leclerc, K. Lee, and A.J.Heeger, *Bulk heterojunction solar cells with internal quantum efficiency approaching 100%*, NATURE PHOTONICS, 3 (2009) 297-303.

[26] W. Ma, C. Yang, X. Gong, K. Lee, A. J. Heeger, Adv. Funct. Mater. 2005,15,1617.

[27] D.A. Case, T.A. Darden, T.E. Cheatham, III, C.L. Simmerling, J. Wang, R.E. Duke, R. Luo, R.C. Walker, W. Zhang, K.M. Merz, B. Roberts, S. Hayik, A. Roitberg, G. Seabra, J. Swails, A.W. Goetz, I. Kolossváry, K.F. Wong, F. Paesani, J. Vanicek, R.M. Wolf, J. Liu, X. Wu, S.R. Brozell, T. Steinbrecher, H. Gohlke, Q. Cai, X. Ye, J. Wang, M.-J. Hsieh, G. Cui, D.R. Roe, D.H. Mathews, M.G. Seetin, R. Salomon-Ferrer, C. Sagui, V. Babin, T. Luchko, S. Gusarov, A. Kovalenko, and P.A. Kollman (2012), AMBER 12, University of California, San Francisco.

[28] J. Fabian and H. Hartmann, *Structure and properties of α-cyclo[N]thiophenes as potential electronic materials-A theoretical study*, J. Phys. Org. Chem. 20 (2007) 554-567.

[29] H. Tamura, I. Burghardt, and M. Tsukada, *Exciton Dissociation at Thiophene/Fullerene Interfaces: The Electronic Structures and Quantum Dynamics*, J. Phys. Chem C.

Acknowledgments

I would like specially to thank Professor Titus Beu for the guidance and for the many fruitful discussions during my PhD research.

I would like to express my thanks to Professor Francesco Zerbetto who supervised my stay at University of Bologna. I also express my thanks to Dr. Siegfried Hoefinger and Dr. Angela Acocella for the consistent help with the molecular dynamics simulations and the electron transfer calculations.

Many thanks to Dr. Aurel Jurjiu for discussions and proof-reading my thesis.

I would like to acknowledge the PhD funding granted through the Sectional Operational Programme for Human Resources Development 2007-2013 co-financed by the European Social Fund, under the project POSDRU 88/1.5/S/60185 - ”Innovative Doctoral Studies in a Knowledge Based Society” and also the CNCSIS-UEFISCSU Project Number PNII-ID PCCE_129/2008.

List of publications

Papers in refreed journals

1. **Sergiu C. Pop**, Titus. A. Beu," Vibrations of polythiophenes", Computational and Theoretical Chemistry 995 66–74 (2012) (previously named J. Mol. Struc.-THEOCHEM)
   ISI: 1.437 / 2 = 0.718
   AIS = 0.305

2. S. Höfinger, A. Acocella, **S. C. Pop**, T. Narumi, K. Yasuoka, T. Beu, and F. Zerbetto, "GPU-Accelerated Computation of Electron Transfer", Journal of Computational Chemistry 33, 2351–2356 (2012).
   ISI: 4.583 / 7 = 0.655
   AIS: 1.518

3. A. Moser, I. Salzmann, M. Oehzelt, A. Neuhold, H.-G. Flesch, J. Ivanco, **S. C. Pop**, T. Toader, D. R. T. Zahn, D.-M. Smilgies, and R. Resel, "A Frozen Smectic State in Thin Films of Sexithiophene", (submitted to Applied Physics Letters).
   ISI: 3.787 / 11 = 0.344
   AIS =1.384

Conference contributions

1. D. Karnaushenko, J. Ivanco, T. Toader, P. Schäfer, **S. C. Pop**, D. Marchenko, A. Firsov, W. Braun, D.R.T. Zahn, "Photoemission studies on the formation of top metallic contacts to organic films", 37^{th} International Conference on Vacuum UltraViolet and X-ray Physics (VUVX2010),11–16 July2010, Vancouver, Canada, poster presentation.

2. **Sergiu C. Pop** and Titus A. Beu, "Vibrations of Polythiophenes", ElecMol10: 5th International Meeting on Molecular Electronics, 6-10 December 2010, Grenoble, France, poster presentation.

3. **S. C. Pop**, T. Beu, S. Hoefinger, A. Acocella, F. Zerbetto, "Electron transfer in organic solar cells", International Conference on Simulation of Organic Electronics and Photovoltaics, 10-14 June 2012, Oliva, Spain, poster presentation.

4. **Sergiu C. Pop** and Titus A. Beu, "Vibrational spectroscopy of thiophene-fullerene dyads", 31^{st} European Congress on Molecular Spectroscopy, 26-31 August 2012, Cluj-Napoca, Romania, poster presentation.